Sagnac mirror loop with two polarization maintaining fibers for twist measurement by tracking adjacent dips with tunable measurement range

Pingsheng Xue[1,2], Qiang Liu[1,2,3*], Qiang Wu[4*], and Richard Fu[4]

1. *College of Information Science and Engineering, Northeastern University, Shenyang 110819, China*
2. *School of Control Engineering, Northeastern University at Qinhuangdao, Qinhuangdao 066004, China*
3. *Hebei Key Laboratory of Micro-Nano Precision Optical Sensing and Measurement Technology, Qinhuangdao 066004, China*
4. *Faculty of Engineering and Environment, Northumbria University, Newcastle upon Tyne NE1 8ST, U.K.*

*Corresponding author.

E-mail address: liuqiang@neuq.edu.cn (Q. Liu), qiang.wu@northumbria.ac.uk (Q. Wu).

ABSTRACT

The transmission characteristics of Sagnac fiber loop interferometer which consists two sections of polarization-maintaining fiber (PMF) spliced at different offset angles were analyzed. Based on the simulation results, an application for twist measurement where PMFs were spliced at different offset angles was designed. When the lengths of two PMFs are equal, a clear spectrum can be obtained for twist or torsion sensing. A phenomenon that the dips would split or merge with twist angle alteration can be used for sensing. Measurement range and sensitivity can be adjusted by changing the PMFs offset angle. The sensitivity was improved by calculating the distance between two adjacent dips, being 0.73 nm/° or 8.37 nm/(rad/m) when the offset angle was 75°.

Keywords: fiber loop interferometer, polarization maintaining fiber, fiber sensor.

1. Introduction

Fiber optic sensors have been widely used in civil engineering, aerospace, biomedicine, and other fields due to their high sensitivity, strong anti-interference ability and good reversibility [1]-[3]. Fiber sensors based on interferometers [4]-[7] are

widely designed because their principles are usually simple and spectrums are clear for observing. There are several types of the fiber interferometers, Fabry–Pérot (F-P) [4], Mach Zehnder (M-Z) interferometers [6], [7], fiber ring resonators [8] and fiber loop (Sagnac) interferometers are the most common. Among them, fiber loop interferometers are usually based on birefringence characteristics of the fibers embedded in the loop, they are polarization independent, both the phase differences and extinction ratio of interference dips can be tuned flexibly.

Fiber loop interferometers have been investigated deeply and widely applied in fiber gyros or sensors. For their advantages of high sensitivity and easy-configuration, a large amount of fiber loop interferometers are designed for sensing. Various parameters such as strain, temperature, refractive index and so on can be measured by fiber loop interferometers with single or multi-section fibers [9]-[14]. The following table lists several fiber loop structures for sensing in recent years:

Table I. Fiber loop interferometers for sensing in recent years

Ref	Interferometer setup	Fiber type	Application
[9]	Cascaded loops	PM-125-03	Strain
[11]	Three HBFs in loop	HBF	Strain, temperature
[12]	Two PMFs in loop, one etched	Panda	Refractive index
[15]	Single loop with low birefringence PCF	LMA-10	Twist
[18]	Two PMFs in loop	PM-1550	Twist
[21]	Two PMFs in loop	PM-1017C	Strain, temperature
[25]	PMF and Multi-core fiber (MCF) in loop	PMF, MCF	Temperature

In fields like industrial manufacturing and civil engineering, twist sensing is critical. Twist measurement can be realized based on fiber loop interferometers as well. In [15] low-birefringence photonic crystal fiber based Sagnac interferometer for twist sensing with sensitivity of 1 nm/° (considering twisted length, the sensitivity was 1.15nm/(rad/m)) was demonstrated, having linear response from 75° to 140°. In [16], a twist sensor based on Sagnac single-mode optic fiber interferometer had the sensitivity of 0.19 nm/° (2.18 nm/(rad/m)) from -45° to 45°. A compact Sagnac loop based on a microfiber coupler for twist sensing with the sensitivity of 0.9 nm/° (3.09 nm/(rad/m)) was designed in [17]. In [18] optical fiber temperature and torsion sensor based on Lyot-Sagnac interferometer was presented, it had very high temperature sensitivity, and it

can realize twist sensing by observing fringe visibility after a fast Fourier-transform.

In this paper, we investigated the sensing characteristics of a fiber loop interferometer which consists two PMFs. The birefringence axis of the two PMFs were spliced with certain angle between them and embedded in the Sagnac interferometer to obtain different transmission spectra. After calculating and analyzing the transmission properties, twist measurements with different offset splice angles were carried out. The wavelength difference between two adjacent dips varies with twist angle, sensitivity is magnified by calculating the distance between the dips. The twist sensitivity was 0.73 nm/° (8.37 nm/(rad/m)), when the offset splicing angle was 75°, which is competitive among previous works, twist from -15° to 15° can be measured. Sensitivity can further increase at the expense of measuring range.

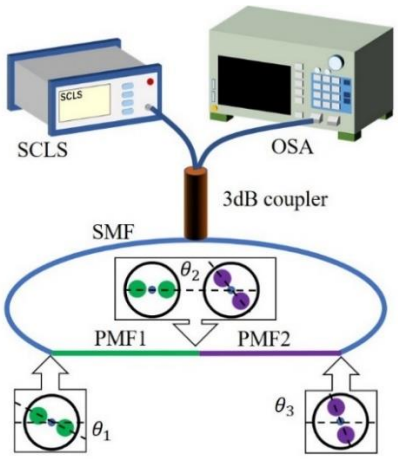

Fig. 1. Schematic of the Sagnac interferometer with two PMFs.

2. Principle

The schematic of Sagnac interferometer with two PMFs is shown in Fig. 1. The light from supercontinuum light source (SCLS) splits up equally at the 3dB coupler and propagates clockwise and counter clockwise in the fiber loop. Phase difference occurs because of the high birefringence of the PMF and causes interference which can be observed on the optical spectrum analyzer (OSA). Fig. 1 insets show the schematic of splicing with angle between two PMF segments in the optical fiber loop, this can be realized by setting the splicing procedure of a polarization maintaining fiber splicer (Fujikura FSM-100P+). In this structure, the transmission properties can be calculated by [18]:

$$\begin{pmatrix} E_{\text{outx}} \\ E_{\text{outy}} \end{pmatrix} = [\mathbf{R}(-\theta_3)\mathbf{M}_{CW}\mathbf{R}(\theta_1) - \mathbf{R}(-\theta_1)\mathbf{M}_{CCW}\mathbf{R}(\theta_3)] \begin{pmatrix} E_{\text{inx}} \\ E_{\text{iny}} \end{pmatrix} \quad (1)$$

In the equation:

$$\mathbf{M}_{CW} = \begin{pmatrix} e^{-\frac{j\varphi_2}{2}} & 0 \\ 0 & e^{\frac{j\rho_2}{2}} \end{pmatrix} \begin{pmatrix} \cos\theta_2 & \sin\theta_2 \\ -\sin\theta_2 & \cos\theta_2 \end{pmatrix} \begin{pmatrix} e^{-\frac{j\varphi_1}{2}} & 0 \\ 0 & e^{\frac{j\varphi_1}{2}} \end{pmatrix};$$

$$\mathbf{M}_{CCW} = \begin{pmatrix} e^{-\frac{j\varphi_1}{2}} & 0 \\ 0 & e^{\frac{j\varphi_1}{2}} \end{pmatrix} \begin{pmatrix} \cos\theta_2 & -\sin\theta_2 \\ \sin\theta_2 & \cos\theta_2 \end{pmatrix} \begin{pmatrix} e^{-\frac{j\varphi_2}{2}} & 0 \\ 0 & e^{\frac{j\varphi_2}{2}} \end{pmatrix};$$

$$\mathbf{R}(\theta) = \begin{pmatrix} \cos\theta & -\sin\theta \\ \sin\theta & \cos\theta \end{pmatrix}; \varphi = 2\pi BL/\lambda.$$

$\mathbf{M}_{CW}$ and $\mathbf{M}_{CCW}$ are Jones matrixes for transmitting in the PMFs clockwise and counterclockwise respectively, where φ_1 and φ_2 are phase differences between fast and slow axes accumulated in each section. θ_2 is the offset angle of two PMFs. θ_1 and θ_3 are the angles between slow axis and x direction on the end faces of PMF1 and PMF2, B represents birefringence and L is the fiber length.

E_{inx}, E_{iny} are the electric field intensities of input from the source, E_{outx}, E_{outy} are output of the interferometer to the OSA. Therefore, the transmittance can be expressed as:

$$T = \frac{|E_{\text{outx}}|^2 + |E_{\text{outy}}|^2}{|E_{\text{inx}}|^2 + |E_{\text{iny}}|^2} \quad (2)$$

According to equation (1), transmittance can be expressed as:

$$T = \left[\sin\theta\cos\theta_2\cos\left(\frac{\pi B(L_1+L_2)}{\lambda}\right) + \cos\theta\sin\theta_2\cos\left(\frac{\pi B(L_1-L_2)}{\lambda}\right)\right]^2 \quad (3)$$

In which, L_1 and L_2 are the lengths of PMF1 and PMF2, $\theta = \theta_1 - \theta_3$. Output spectrum is associated with θ_2, θ and L_1, L_2. Twist sensing can be realized.

3. Results and discussion

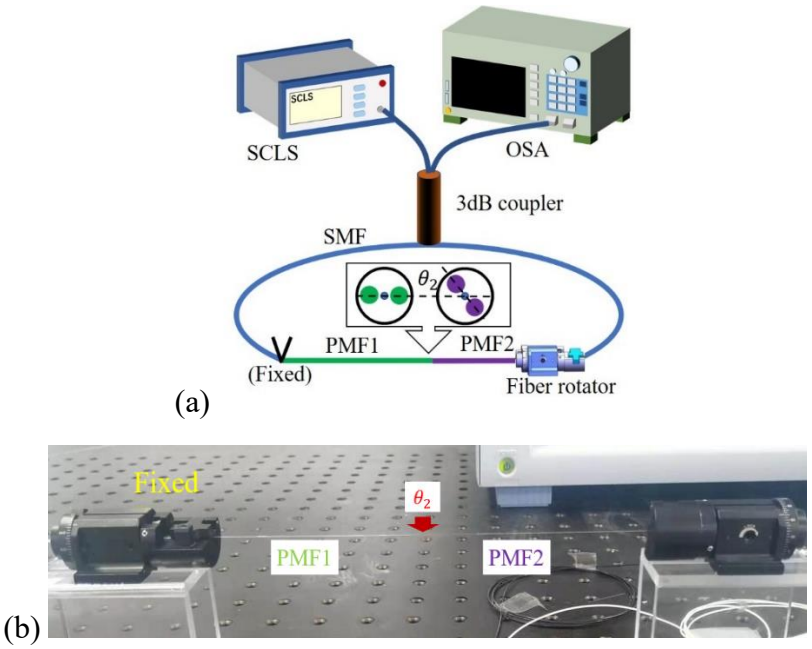

Fig. 2. (a) Experiment schematic for twist measurement. (b) Setup of the sensing section.

I. Simulation analysis

In this section, we analyze the spectrum characteristics, especially the variation trend of the interference dips. When PMF1 and PMF2 are spliced with 45° between their birefringence axes ($\theta_2 = 45°$) on the end faces, the other end of PMF1 is fixed and the end of PMF2 can be rotated by a fiber rotator to adjust θ_3 (Fig. 2). In this case, θ_2 is constant, θ is variable due to varying θ_3. The birefringence of the PMF was set to 0.00045 in calculation, this value is very close to the exact value of the PMF we used (SM-15-PS-U25D, Fujikura; diameter 125μm), and the dispersion was neglected. Firstly, the lengths of two fibers are considered, when two fibers are in different lengths, it always results in forming envelope. Envelopes can magnify strain or temperature sensitivities, but envelopes are not expected by us in this case. Envelopes usually have large full width at half maxima, and the shifts of envelopes are hard to be directly observed. According to equation (3), when their lengths are equal, equation can be further simplified into $T = [\sin\theta\cos\theta_2\cos(\pi B(L_1 + L_2)/\lambda) + sin\theta_2\, cos\theta]^2$ spectrum will be rather clear and regular. Fig. 3 shows different fiber length ratios between PMF1 and PMF2, when it is 1:1, the spectrum has less dips, which will make it easier to read and track the spectrum in sensing application. For the dips position, which can be solved by making dT/dλ=0, that is:

$$\lambda = \pi B(L_1 + L_2)/[(2k+1)\pi \pm arccos\left(\frac{tan\theta_2}{tan\theta}\right)] \quad (4)$$

In which, k is an integer, $\pi - \theta_2 > \theta > \theta_2$, $\theta_2 < 90°$. When PMF1 and PMF2 are both 10 cm, the calculated transmission is shown in Fig. 4. The Dip A and B become more obvious when θ changes from 0° to 45°, and the dips are most obvious when θ reaches 45°. Then the dips split up as the angle continues increasing, Dip A splits into Dip A1 and A2, so does B into B1 and B2, Dip A1 and B1 blue shift while A2 and B2 red shift. When θ reaches 90°, the gap between dips become uniform and the free spectrum range (FSR) is half of that when θ is 45°. Dip A1 and B2 merged into Dip C when θ = 135° and then the extinction ratio of Dip C decreases as the angle continues increasing.

With the characteristics above, twist measuring can be realized by tracking the splitting dips. According to equation (4) the distance between two adjacent splitting dips, $\lambda_2 - \lambda_1$, can be expressed as:

$$\lambda_2 - \lambda_1 = \frac{2\pi BL\, arccos\left(\frac{tan\theta_2}{tan\theta}\right)}{[(2k+1)\pi + arccos\left(\frac{tan\theta_2}{tan\theta}\right)][(2k+1)\pi - arccos\left(\frac{tan\theta_2}{tan\theta}\right)]} \quad (5)$$

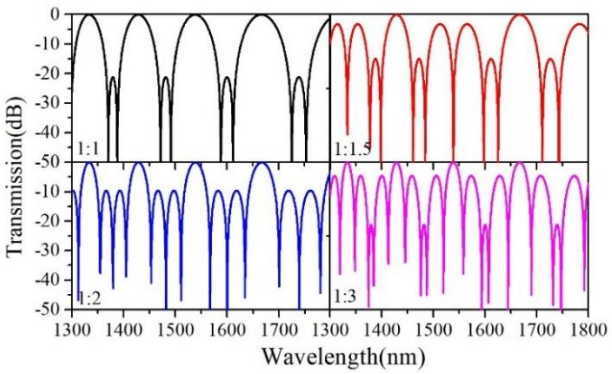

Fig. 3. Calculated results for different fiber length ratios of PMF1:PMF2, $\theta_2 = 45°$.

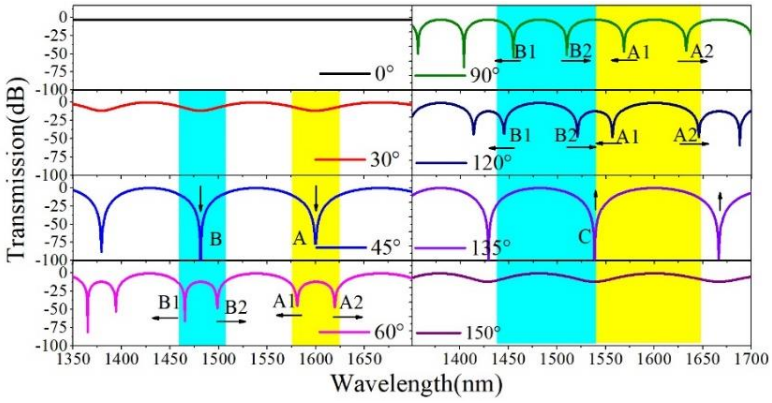

Fig. 4. Calculated results of the spectrum when $\theta_2 = 45°$, θ varies from 0° to 150°. Arrows mark the variation trend of the spectrum.

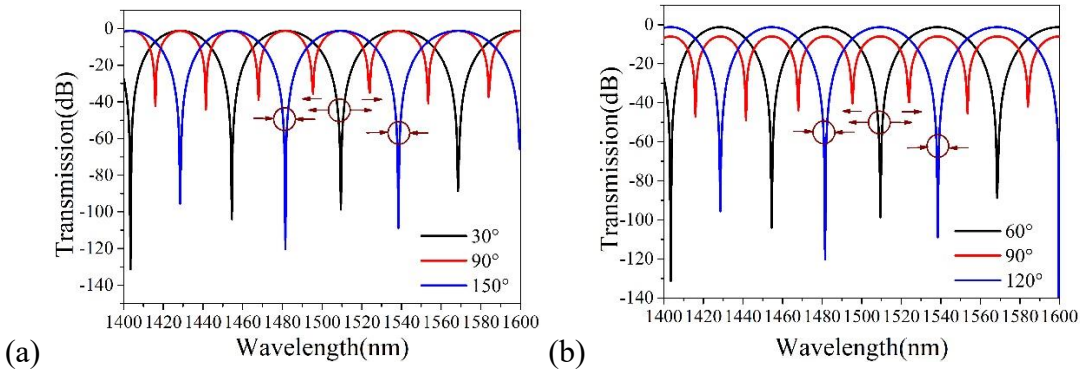

Fig. 5. Calculated spectrum for (a) $\theta_2 = 30°$, dips split when $\theta = 30°$ and merge when θ=150° and (b) $\theta_2 = 60°$, dips split when $\theta = 60°$ and merge when $\theta = 120°$.

While $\theta_2 = 30°$, it can be seen from the simulated spectrum, the dips will split at $\theta = 30°$, move away from each other and merge with next dip at $\theta = 150°$ (Fig. 5(a)). For $\theta_2 = 60°$, dips will split at $\theta = 60°$ and merge at $\theta = 120°$ (Fig. 5(b)). It can be concluded from equation (3) and simulated results that dips will split up at $\theta = \theta_2$ and merge with next dip at $\theta = \pi - \theta_2$.

II. Experiment and results

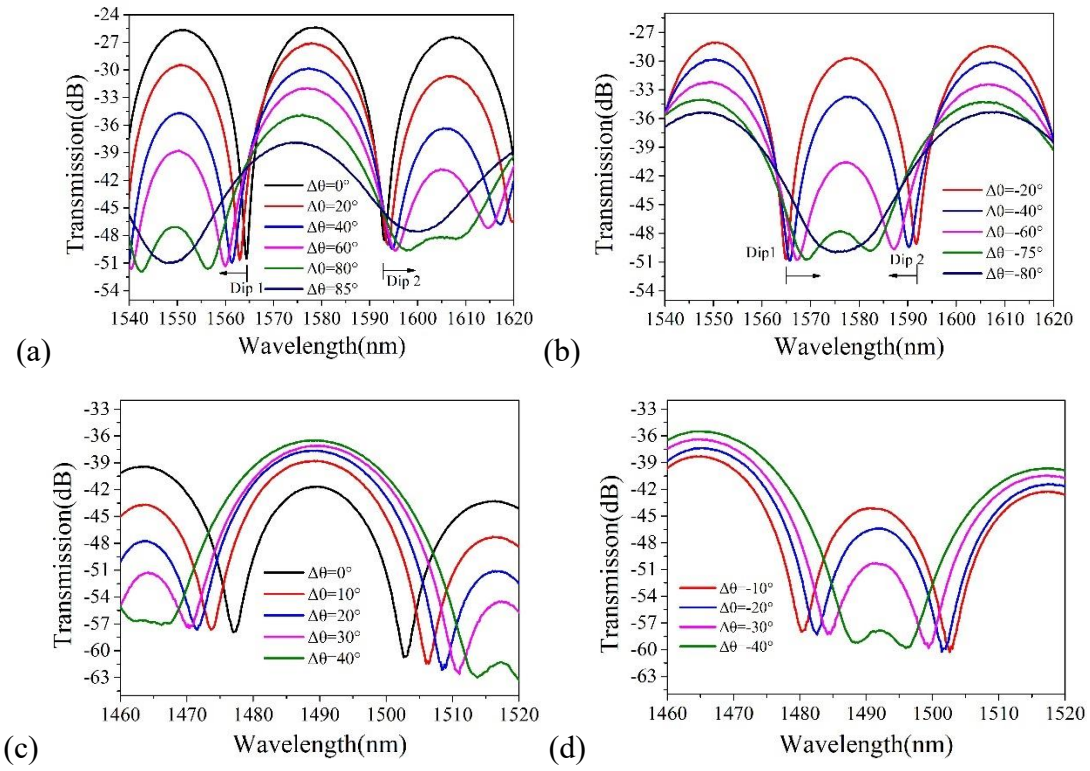

Fig. 6. Initial position is set as $\theta = 90°$ (FSR is uniform), $\Delta\theta$ represents the twisted angle from the initial position. Spectrum in experiment when $\theta_2 = 30°$, (a) the two dips we considered come close to each other when it was twist in one direction, (b) while they move away from each other when twisted in the other direction. (c, d) When $\theta_2 = 60°$, spectrum responses in both directions.

With the characteristics above, twist measuring can be realized by tracking the splitting dips. By setting $\theta = 90°$ at initial position to obtain the most uniform gaps among dips, dual twist direction detection can be realized, the measuring range can be adjusted by setting θ_2. When the fiber suffers twist, adjacent dips will move in opposite directions. Dip A1 and B2 will move close to each other when the fiber suffers twist in one direction and move away from each other in the other direction. Fig. 6(a) shows twisting test when $\theta_2 = 30°$, starting twist the fiber from initial position, Dip1 blue shifted and Dip2 red shifted, the space between them was increasing as twisted angle increased, while Dip1 red shifted and Dip2 blue shifted and the space was decreasing when the fiber was twisted in the other direction (Fig. 6(b)). Theoretically, the twisted angle $\Delta\theta$ of $\pm 60°$can be measured when $\theta_2 = 30°$. But in experiment $\Delta\theta$ were -80° and +85° due to errors which come from the fixing of θ_1, torsion of the SMF in the loop and slight fiber length difference when the PMF was cleaved. When $\theta_2 = 60°$, the

spectrum of different twist angles are plotted in Fig. 6(c)(d). Response range is from -40° to 40°.

The relation between twisted angle and wavelength difference between Dip1 and Dip2 ($\lambda_2 - \lambda_1$) is plotted in Fig. 7. The sensitivity is magnified if their distance $\lambda_2 - \lambda_1$ was calculated instead of tracking the wavelength shift of only one dip. According to Fig. 7(a), when $\theta_2 = 30°$, a fitted result with linearity of 0.9898 can be obtained in a limited measuring range from -40° to 60° and the sensitivity is 0.11nm/° (considering the length of both PMFs was 10 cm, the torsion sensitivity can be expressed as 1.26 nm/(rad/m)). When $\theta_2 = 45°$, the sensitivity is 0.27 nm/° (3.09 nm/(rad/m)) with the linearity of 0.9972 from -35° to 35° (Fig. 7(b)). While $\theta_2 = 60°$, -30° to 30° can be measured with sensitivity of 0.44 nm/°(5.04 nm/(rad/m)) and linearity of 0.9868 (Fig. 7(c)). The sensitivity reached 0.73 nm/°(8.37 nm/(rad/m)) in range from -15° to 15° when θ_2 was set as 75° (Fig. 7(d)). In the whole ranges, the responses conform to arccos(tan$x$) functions, which is consistent with equation (5).

By adjusting θ_2, response range can be tuned at the expense of sensitivity, the larger θ_2, the higher sensitivity, but the range can be measured is smaller. However, for measuring tiny twist deformation of an object in application, the range is not a problem of concern. According to equation (5), $(2k + 1)\pi$ is a much larger number, so the denominator can be considered as a constant approximating $[(2k + 1)\pi]^2$. When torsion is applied, for the same twisted angle, $\lambda_2 - \lambda_1$ will be larger (when $\theta > 90°$) or smaller (when $\theta < 90°$) if θ_2 is larger. That explains larger θ_2 will result in higher sensitivity. Since integer k is relative with L and approximately proportion to it, from the equation we can estimate, shorter fiber results in higher sensitivity of 'nm/°'(total twisted angle), but for sensitivity of 'nm/(rad/m)'(twisted angle per meter), the fiber length hardly has influence on the sensitivity. Factors such as temperature may usually have influence on the sensing performance. Fig. 8 plots the temperature response of this structure, all dips shifted to left as temperature increasing. By tracking one dip, the sensitivity is about 0.7 nm/°C, while it can be compensated to less than 0.2 nm/°C by calculating $\lambda_2 - \lambda_1$. Calculating the distance of adjacent dips can mitigate the influence of strain or temperature which usually cause dips drift in the same direction to some extent [11], [20]. Or if needed, double quantity simultaneous sensing can be realized by

constructing matrixes [11], [21]. Meanwhile it is more stable to track dips compared with works which transmission intensities were observed [18], [22]-[24] because light source energy fluctuation has no influence on the dip wavelengths.

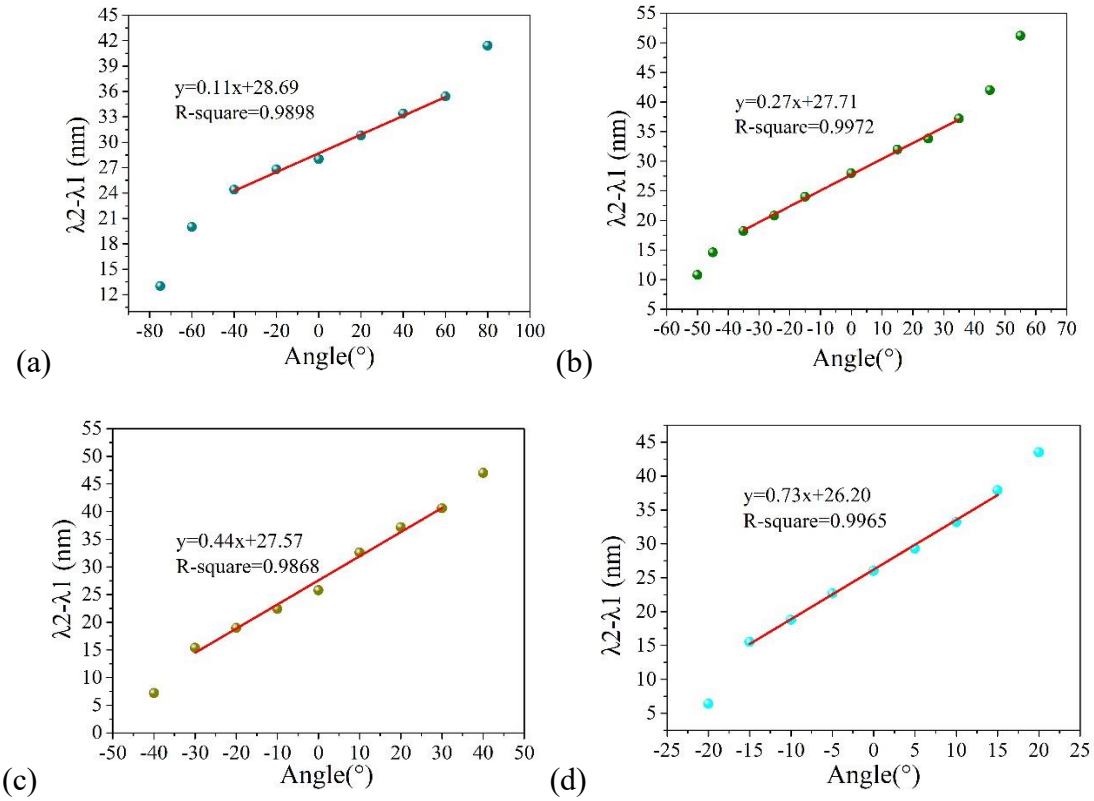

Fig. 7. Responses and fitting results for (a) $\theta_2 = 30°$, (b) $\theta_2 = 45°$, (c) $\theta_2 = 60°$ and (d) $\theta_2 = 75°$. In limited ranges around the initial position, the responses are in good linearity, in large scale, they conform to arctan function responses.

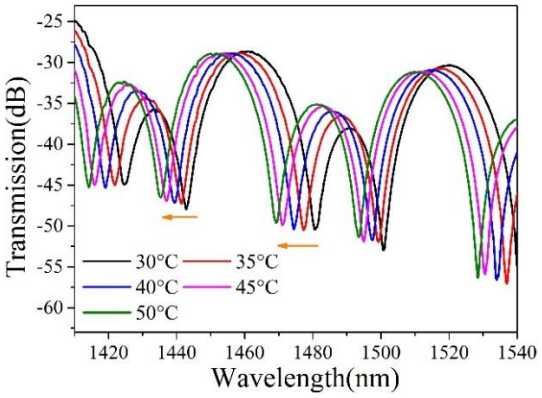

Fig. 8. All dips shifted in the same direction as temperature varies, calculating $\lambda_2 - \lambda_1$ will mitigate the influence of temperature to some extent.

4. Conclusions

The transmission characteristics of the Sagnac interferometer which consists two sections of PMF were investigated. When the two sections of PMF were spliced together with a certain angle between their birefringence axes, the sensing characteristics for twist sensing were discussed. The method for twist sensing was proposed, by observing the gap between two adjacent dips, the sensitivity was improved. The twist measurement range can be tuned by adjusting the offset angle (θ_2) between two PMFs and reducing the measurement range will result in higher sensitivity. The response was relatively linear from -15° to +15° when $\theta_2 = 75\,^{\circ}$ and the sensitivity was 0.73 nm/°(8.37 nm/(rad/m)). The device is easy to fabricate, low in cost and can be widely applied in twist/torsion sensing field.

Acknowledgments

This research was funded by the National Natural Science Foundation of China (Grant No. 51907017), the Key Science and Technology Research Projects of Higher Education Institutions in Hebei Province of China (Grant No. ZD2019304), Hebei Natural Science Foundation (Grant No. F2020501040), the Fundamental Research Funds for the Central Universities of China (Grant No. N2123012).

References

[1] Y. Monfared, C. Liang, and R. Khosravi, et al. Selectively toluene-filled photonic crystal fiber Sagnac interferometer with high sensitivity for temperature sensing applications. Results Phys, vol. 13, 102297. 2019.
[2] F. Jos, C. Dimitrios, T. Alberto, et al. Infiltrated photonic crystal fibers for sensing applications. Sensors-Basel, vol.18, no.12, 4263, 2018.
[3] Y. Zhao, R. Tong, F. Xia, et al. Current status of optical fiber biosensor based on surface plasmon resonance. Biosens. Bioelectron, vol. 142, 111505, 2019.
[4] L. Cai, J. Wang, M. Chen, X. Ai, A High-sensitivity strain sensor based on an Unsymmetrical air-microbubble Fabry-Perot interferometer with an ultrathin wall. Measurement, vol. 181, 109651, 2021.
[5] X. Li, Y. Zhao, X. Zhou, and L. Cai, High sensitivity all-fiber Sagnac interferometer temperature sensor using a selective ethanol-filled photonic crystal fiber, Instrum. Sci. Technol. vol. 46, no. 3, pp. 253-264, 2018.
[6] W. Yuan, Q. Zhao, L. Li, Y. Wang, and C. Yu, Simultaneous measurement of temperature and curvature using ring-core fiber-based Mach-Zehnder interferometer. Opt. Express, vol. 29, no. 12, pp. 17915-17925, 2021.
[7] S. Yan, Y. Zhao, M. Chen and Q. Liu, Optical fiber strain sensor with double S-tapers. Instrum. Sci. Technol., vol. 49, no. 3, pp. 313-326, 2021.

[8] L. Cai, F. Xia, H. Zhang, and Y. Zhao, Temperature sensing characteristics of an MKR in a microfiber taper based on mechanisms of interference and resonance with vernier effect, Opt. Laser Eng., vol. 143, 106617, 2021.
[9] Q. Liu, L. Xing, Z. Wu, Y. Fu, S. Li, P. Xue, W. Ng, Q. Wu, and R. Binns, Cascaded Sagnac loops embedded with two polarization maintaining photonic crystal fibers for highly sensitive strain measurement. IEEE T. Instrum. Meas, vol. 70, pp. 1-9, 2021.
[10] G. Sun, D. Moon, and Y. Chung. Simultaneous temperature and strain measurement using two types of high-birefringence fibers in Sagnac loop mirror. IEEE Photonics Technol. Lett., vol. 19, no. 24, 2007.
[11] G. Sun, H. Tang, Y. Hu, and Y. Zhou. Strain and temperature discrimination using high birefringence fiber Sagnac interferometer with enhanced sensitivities. IEEE Photonics Technol. Lett., vol. 24 no. 7, 2012.
[12] C. Zhong, C. Shen, Y. You, J. Chua, X. Zou, X. Dong, Y. Jin, J. Wang, A polarization-maintaining fiber loop mirror based sensor for liquid refractive index absolute measurement. Sensor Actuat. B-Chem., vol. 168, pp. 360-364, 2012.
[13] S. Liu, P. Lu, E. Chen, W. Ni, D. Liu, J. Zhang, and Z. Lian. Vernier effect of fiber interferometer based on cascaded PANDA polarization maintaining fiber Chin. Opt. Lett., vol. 17, no. 8, 080601, 2019.
[14] D. Leandro, M. Bravo and M. Lopez-Amo, High resolution polarization-independent high birefringence fiber loop mirror sensor. Opt. Express, vol. 23, no. 14, 249263, 2015.
[15] P. Zu, C. Chan, Y. Jin, T. Gong, Y. Zhang, L. Chen, and X. Dong, A temperature-insensitive twist sensor by using low-birefringence photonic-crystal-fiber-based Sagnac interferometer. IEEE Photonic Technol. Lett. vol. 23, no. 13, pp. 920-922, 2011.
[16] H. Liang, M. Sun, Y. Jin, Twist sensor based on Sagnac single-mode optic fiber interferometer. Optik, vol. 124, pp. 6676-6678, 2013.
[17] Y. Chen, Y. Semenova, G. Farrell, F. Xu, and Y. Lu, A compact Sagnac loop based on a microfiber coupler for twist sensing. IEEE Photonics Technol. Lett., vol. 27, no. 24, pp. 2579-2582, 2015.
[18] L. Shao, X. Zhang, H. He, Z. Zhang, X. Zou, B. Luo, W. Pan and L. Yan. Optical fiber temperature and torsion sensor based on Lyot-Sagnac interferometer, Sensors-Basel, vol. 16, 1774, 2016.
[19] Y. Liu, B. Liu, X. Feng, W. Zhang, G. Zhou, S. Yuan, G. Kai, and X. Dong. High-birefringence fiber loop mirrors and their applications as sensors. Appl. Optics, vol. 44, no. 12, pp. 2382-2390, 2005.
[20] C. Shen, C. Zhong, J. Chu, X. Zou, Y. Jin, J. Wang, X. Dong, Y. Li, and L. Wang. Temperature-insensitive strain sensor using a fiber loop mirror based on low-birefringence polarization-maintaining fibers. Opt. Commun., vol. 287, pp. 31-34, 2013.
[21] S. Xiao, B. Wu, Y. Dong, H. Xiao, S. Yao, and S. Jian. Strain and temperature discrimination using two sections of PMF in Sagnac Interferometer. Opt. Laser Technol., vol. 113, pp. 394-398, 2019.
[22] T. Hu, Y. Zhao and D. Wu, Novel torsion sensor using a polarization maintaining photonic crystal fiber loop mirror. Instrum. Sci. Technol., vol. 44, pp. 46-53, 2016.
[23] B. Huang and X. Shu, Highly sensitive twist sensor based on temperature- and

strain-independent fiber Lyot filter. IEEE J. Lightwave Technol. vol. 35, no. 10, pp. 2026-2031, 2017.
[24] C. Jiang, Y. Liu,Y. Zhao, C. Mou and T. Wang, Helical long-period gratings inscribed in polarization-maintaining fibers by CO_2 laser. IEEE J. Lightwave Technol., vol.37, no. 3, pp. 889-896, 2018.
[25] F. Zhang, Y. Yue, and J. Hu, Highly sensitive temperature sensor based on multicore fiber-polarization maintaining fiber loop mirror. IEEE Sens. J., vol. 20, no.3, pp. 1315-1321, 2020.